

Baryon-density dependence of viscosities of the quark-gluon plasma at hadronization

Zhidong Yang , Yifeng Sun, and Lie-Wen Chen *

School of Physics and Astronomy, Shanghai Key Laboratory for Particle Physics and Cosmology, and Key Laboratory for Particle Astrophysics and Cosmology (MOE), Shanghai Jiao Tong University, Shanghai 200240, China



(Received 2 November 2023; revised 25 March 2024; accepted 17 April 2024; published 9 May 2024)

The ϕ meson and Ω baryon provide unique probes of the properties of the quark-gluon plasma (QGP) at hadronization in relativistic heavy-ion collisions. Using the quark recombination model with the quark phase-space information parameterized in a viscous blast wave, we perform Bayesian inference of the shear and bulk viscosities of the QGP at hadronization with a temperature of $T \approx 160$ MeV by analyzing the ϕ and Ω data in Au+Au collisions at $\sqrt{s_{NN}} = 19.6$ –200 GeV and Pb+Pb collisions at $\sqrt{s_{NN}} = 2.76$ TeV, corresponding to a baryon chemical potential variation from $\mu_B \approx 0$ (at $\sqrt{s_{NN}} = 2.76$ TeV) to 200 MeV (at $\sqrt{s_{NN}} = 19.6$ GeV). We find that the shear viscosity to enthalpy ratio $\eta T/(\epsilon + P)$ of the QGP at hadronization decreases as μ_B increases, with $\eta T/(\epsilon + P) \approx 0.18$ at $\mu_B = 0$ and $\eta T/(\epsilon + P) \approx 0.08$ at $\mu_B = 200$ MeV, while the corresponding specific bulk viscosity is essentially constant with $\zeta T/(\epsilon + P) = 0.02$ –0.04 for $\mu_B < 200$ MeV. Our results suggest that the QGP at hadronization ($T \approx 160$ MeV) with finite baryon density is more close to perfect fluid than that with zero baryon density.

DOI: [10.1103/PhysRevC.109.054907](https://doi.org/10.1103/PhysRevC.109.054907)

I. INTRODUCTION

Lattice quantum chromodynamics (QCD) calculations predict a transition from ordinary hadronic matter to a new state of matter that consists of deconfined quarks and gluons, called quark gluon plasma (QGP) [1]. The QGP is believed to have existed in the early universe $10^{-6}s$ after the big bang and can be created in relativistic heavy-ion collisions (HICs) at the BNL Relativistic Heavy Ion Collider (RHIC) and the CERN Large Hadron Collider (LHC). Exploring the QCD phase diagram as well as the transport properties of the QGP is one of the most fundamental problems in high-energy nuclear physics (see, e.g., Ref. [2]). It is known that at zero baryon density or baryon chemical potential ($\mu_B = 0$), the transition between QGP and hadronic matter is a smooth crossover [3,4]. Further calculations from lattice QCD suggest that the crossover line extends up to $\mu_B \approx 250$ –300 MeV [5]. However, it is not yet known if there exists a critical point where the crossover transforms into a first-order phase transition at higher baryon densities. In fact, the main goal of the beam energy scan (BES) program at RHIC is to investigate the phase diagram of QCD and locate the critical point [6].

One of the most significant discoveries made at RHIC and LHC is that the QGP behaves like a near-perfect fluid, characterized by an exceptionally small shear viscosity to entropy density ratio η/s , close to the universal lower bound $1/4\pi$ based on the anti-de Sitter/conformal field theory (AdS/CFT) correspondence [7]. This is surprising since the QGP was initially expected to be a weakly interacting gas of quarks

and gluons but turned out to be a strongly coupled fluid. This discovery has attracted intense interest in the transport properties of the QGP fluid, which are closely related to the underlying strong interactions between quarks and gluons. In recent years, theoretical calculations on the shear (η) and bulk (ζ) viscosities have been extensively explored [8–19], usually considering $\mu_B = 0$ and focusing on the temperature dependence of viscosities.

The viscosities of the QGP have significant effects on the final observables of HICs [20,21], allowing us to constrain their values with experimental data. Earlier studies employing viscous hydrodynamics usually assumed a constant η/s over the entire evolution and found $\eta/s = 0.08$ –0.2 [22–25]. Recent research using Bayesian statistical analysis with multistage models that integrate initial conditions, viscous hydrodynamics, and hadronic transport obtained constraints on the temperature dependence of the shear and bulk viscosities of the baryon-free QGP [26–36]. Overall, most recent analyses have yielded consistent results and found $\eta/s \approx 0.16$ at pseudocritical temperature $T_{pc} \approx 160$ MeV for the baryon-free QGP [33,36].

Studies have also found that the viscosities of QCD matter depend on baryon chemical potential [18,19,37–40]. By assuming a constant value of η/s for each collision energy, hybrid models that incorporate hadronic transport and viscous hydrodynamics show that different values of effective shear viscosity are required to describe the data at different collision energies [41,42]. The baryon chemical potential dependence of η/s is explored in Refs. [43–45]. In general, due to large uncertainties in the initial conditions and equation of state, hydrodynamics simulations at finite μ_B are under development [43,45–48] and a quantitative estimate for QGP's viscosities at finite μ_B is still challenging.

*Corresponding author: lwchen@sjtu.edu.cn

In this work, we present a novel approach to constrain the shear and bulk viscosities of QGP at finite μ_B with a temperature of $T \approx 160$ MeV by using the ϕ meson and Ω baryon observables in relativistic HICs from LHC to RHIC-BES energies. We find that the QGP at $T \approx 160$ MeV with finite baryon density is more close to perfect fluid than that with zero baryon density. The similar approach has been recently applied to explore the viscosities of the baryon-free QGP at hadronization [49]. In our approach, hadrons are produced through quark recombination [50–59] with the phase-space distribution of quarks at hadronization parameterized in a viscous blast wave [20,60–63], which includes nonequilibrium deformations of thermal distributions due to shear and bulk stresses. The viscous effects for the QGP at hadronization are then imported into ϕ and Ω through the recombination process. Since the ϕ and Ω have relatively small hadronic interaction cross sections [64], they thus carry direct information of QGP at hadronization with negligible hadronic effects [64–72]. It should be pointed out that blast wave models obtain their parameters through fits to data and are independent of initial conditions and equation of state, thus providing a complementary way to hydrodynamic simulations [61,62].

The paper is organized as follows. In Sec. II, we introduce the models and methods employed in our present work. In Sec. III, we present the results and discussions, and the conclusion is given in Sec. IV.

II. MODEL AND METHODS

A. Theoretical model

Quark recombination or coalescence models were initially proposed to explain the baryon-over-meson enhancement and valence quark number scaling observed in RHIC Au+Au collisions [50–56]. In a recent work [49], we introduce viscous corrections into quark recombination, and here give a brief overview of the formalism. In the following \mathbf{r} is the three-space position, \mathbf{p} is the three-momentum, and m is particle mass. The four-momentum of hadrons are denoted as $p^\mu = (E, \mathbf{p})$ with $E = \sqrt{m^2 + p^2}$. Following Refs. [52,53,57], the momentum distribution of mesons is given by

$$E \frac{dN_M}{d^3\mathbf{p}} = C_M \int_\sigma \frac{p^\mu \cdot d\sigma_\mu}{(2\pi)^3} \int_0^1 dx_1 dx_2 \Phi_M(x_1, x_2) \times f_a(\mathbf{r}, x_1\mathbf{p}) f_b(\mathbf{r}, x_2\mathbf{p}). \quad (1)$$

where C_M is the spin degeneracy factor of a given meson species, σ is the hypersurface of hadronization, Φ_M is the effective wave function squared of mesons, $x_{1,2}$ are light cone coordinates defined as $\mathbf{p}_{1,2} = x_{1,2}\mathbf{p}$, and $f_{a,b}$ are the parton phase-space distributions. The Φ_M is parameterized as Gaussian type $\Phi_M \sim \exp(-\frac{(x_1-x_a)^2 + (x_2-x_b)^2}{\sigma_M^2}) \delta(x_1 + x_2 - 1)$, where σ_M is the variance, $x_{a,b} = m_{1,2}/(m_1 + m_2)$ are the peak values, and $m_{1,2}$ are the masses of the constituent partons. A similar expression can be derived for baryons.

The quark phase-space distribution is parameterized in a viscous blast wave [61–63], based on the Retiere and Lisa blast wave [73]. The quark distribution is given by

$$f(r, p) = f_0(r, p) + \delta f_{\text{shear}}(r, p) + \delta f_{\text{bulk}}(r, p), \quad (2)$$

where $f_0(r, p) = 1/(e^{(u^\mu p_\mu - \mu_i)/T} \mp 1)$ is the equilibrium Bose/Fermi distribution as a function of the flow field u^μ , particle momentum p^μ , the local temperature T and chemical potentials $\mu_i = b_i \mu_B + s_i \mu_S + q_i \mu_Q$ with baryon number b_i , strangeness s_i , and electric charge q_i (we assume $\mu_Q = 0$ in this work). δf_{shear} and δf_{bulk} denote corrections from the shear and bulk viscosities, respectively. For the shear viscous corrections, we use the Grad's method [74,75]

$$\delta f_{\text{shear}} = \frac{1}{2T^2} \frac{P_\mu P_\nu}{\epsilon + P} \pi^{\mu\nu} f_0(1 \pm f_0), \quad (3)$$

where ϵ is the energy density, P is the pressure, $\pi^{\mu\nu}$ is the shear stress tensor and $+$ ($-$) for bosons (fermions). In the Navier-Stokes approximation $\pi^{\mu\nu} = 2\eta\sigma^{\mu\nu}$ where η is the shear viscosity and $\sigma^{\mu\nu}$ is the shear gradient tensor defined as $\sigma^{\mu\nu} = \frac{1}{2}(\nabla^\mu u^\nu + \nabla^\nu u^\mu) - \frac{1}{3}\Delta^{\mu\nu}\nabla_\lambda u^\lambda$ with flow field u^μ , $\nabla^\mu = \Delta^{\mu\nu}\partial_\nu$, and $\Delta^{\mu\nu} = g^{\mu\nu} - u^\mu u^\nu$. The spatial derivatives in $\sigma^{\mu\nu}$ can be obtained directly. The time derivatives cannot be given by blast wave itself, and are determined by solving ideal hydrodynamics [63].

For the bulk viscous corrections, we use the 14-moment approximation [76,77]

$$\delta f_{\text{bulk}} = -f_0(1 \pm f_0) \Pi \frac{\tau_\Pi}{\zeta} \left[\frac{1}{3} \frac{m^2}{T} \frac{1}{p^\mu u_\mu} + \frac{p^\mu u_\mu}{T} \left(c_s^2 - \frac{1}{3} \right) \right], \quad (4)$$

where ζ is the bulk viscosity, Π is the bulk viscous pressure, τ_Π is the bulk relaxation time, and c_s^2 is the velocity of sound squared. At the first-order approximation, one has $\Pi = -\zeta \partial_\mu u^\mu$. Following Ref. [76], the ratio of bulk viscosity to bulk relaxation time is given by

$$\frac{\zeta}{\tau_\Pi} = \left(\frac{1}{3} - c_s^2 \right) (\epsilon + P) - \frac{2}{9} (\epsilon - 3P) - \frac{m^4}{9} L_{-2,0} \quad (5)$$

with $L_{-2,0}$ defined as $L_{-2,0} = \frac{g}{(2\pi)^3} \int \frac{d^3\mathbf{p}}{E} \frac{f_0(r,p)}{(p^\mu u_\mu)^2}$ and g the degeneracy factor. We note that the fluidity of a system at finite chemical potential should be evaluated by the ratio of shear viscosity over the enthalpy multiplied by the temperature, $\eta T/(\epsilon + P)$ [78], where $\epsilon + P = Ts + \mu_B n_B$. When $\mu_B = 0$, this quantity reduces to η/s .

Let us now describe the blast-wave parametrization for the flow field u^μ . Here $R_{x,y}$ are the semi-axes of the fireball at freezeout, $\rho = \sqrt{x^2/R_x^2 + y^2/R_y^2}$ is the reduced radius, $\eta_s = \frac{1}{2} \ln \frac{t+z}{t-z}$ is the space-time rapidity. The hypersurface is assumed to be constant $\tau = \sqrt{t^2 - z^2}$. The flow field is parameterized as

$$u^\mu = (\cosh \eta_s \cosh \eta_T, \sinh \eta_T \cos \phi_b, \sinh \eta_T \sin \phi_b, \sinh \eta_s \cosh \eta_T), \quad (6)$$

where η_T is the transverse flow rapidity and ϕ_b is the azimuthal angle of u^μ in the transverse plane. η_T is given by the transverse velocity $v_T = \tanh \eta_T$ with

$$v_T = \rho^n (\alpha_0 + \alpha_2 \cos 2\phi_b), \quad (7)$$

where α_0 is the average surface velocity, α_2 is an elliptic deformation of the flow field, and n is a power term. In this work, we use a linear expression and set $n = 1$. The

TABLE I. Experimental data of ϕ and Ω used in our analysis. Values in parentheses are centralities of Ω when they are different from ϕ .

$\sqrt{s_{NN}}$ (GeV)		Centrality
19.6, 39	$v_2(p_T)$	0–10 %, 10–40 %, 40–80 % [81–83]
	$\frac{dN}{d^2p_T dy}$	0–10 %, 20–30 % (20–40 %), 40–60 % [84,85]
54.4, 62.4	$v_2(p_T)$	0–10 %, 10–40 %, 40–80 % [81,86]
	$\frac{dN}{d^2p_T dy}$	0–20 %, 20–40 %, 40–60 % [87,88]
200	$v_2(p_T)$	0–30 %, 30–80 % [89]
	$\frac{dN}{d^2p_T dy}$	10–20 % (0–5 %), 40–50 % (40–60 %) [90,91]
2760	$v_2(p_T)$	10–20 %, 20–30 %, 30–40 %, 40–50 % [92,93]
	$\frac{dN}{d^2p_T dy}(\phi)$	
	$\frac{dN}{d^2p_T dy}(\Omega)$	10–20 %, 20–40 %, 40–60 % [94]

transverse flow vector is chosen to be perpendicular to the elliptic surface at $\rho = 1$. The ratio R_y/R_x significantly influences elliptic flow, so we choose R_y/R_x as a fit parameter and constrain R_x , R_y , and τ by adding a simple geometric estimate $R_x \approx (R_0 - b/2) + 0.65\tau(\alpha_0 + \alpha_2)$ where R_0 is the radius of the colliding nucleus and b is the impact parameter. The values of b used for each centrality bin are based on Glauber Monte Carlo simulations for related experiments [79,80].

It should be noted that the viscous blast wave offers a simplified representation of the flow field and freezeout hypersurface, serving as an approximate snapshot of a viscous hydrodynamic system at a fixed time [20,60–63]. The dissipative effects before freezeout are effectively incorporated into the parameterized flow field u^μ . Consequently, the viscous blast wave carries information on the viscosities of the fluid at a specific time, e.g., the QGP at hadronization in our present work.

B. Experimental data and fit parameters

We utilize the transverse-momentum (p_T) spectra and elliptic flows v_2 of ϕ and Ω as our observables. The data we used are from the STAR Collaboration, covering Au+Au collisions at 19.6, 39, 54.4, 62.4, and 200 GeV [81–91] (STAR preliminary data for v_2 at 19.6 GeV), and the ALICE Collaboration for Pb+Pb collisions at $\sqrt{s_{NN}} = 2.76$ TeV [92–94] around midrapidity, as listed in Table I. Due to data availability, the centrality bins for spectra are slightly different from that of v_2 . For Au+Au at 19.6, 39, 54.4, and 62.4 GeV, we use data of Ω^- . For Au+Au at 200 GeV and Pb+Pb at 2.76 TeV, we use data of $\Omega^- + \bar{\Omega}^+$. For Au+Au collisions at $\sqrt{s_{NN}} = 7.7, 11.5, \text{ and } 27$ GeV, the current data of ϕ and Ω have very few points and large uncertainties, so we will not use them in our analysis. As for the spectra of ϕ and Ω at $\sqrt{s_{NN}} = 54.4$ GeV, there is currently no available data and we use the spectra from $\sqrt{s_{NN}} = 62.4$ GeV instead.

For each collision energy, we perform a combined analysis of the available centrality bins. The fitted p_T ranges for ϕ and Ω are given in Table II. We have checked that the correction $\delta f(r, p)$ is small for both ϕ and Ω with the above fit ranges, i.e., less than 20% of f_0 for the majority of points (very few points going up to 40% of f_0), which is much smaller than

the commonly adopted upper bound ≈ 1 [20,30], ensuring the applicability of the viscous corrections.

The temperature T and baryon chemical potentials μ_B at hadronization are taken from Ref. [95], by assuming their values are close to the corresponding values at chemical freezeout for different collision energies. Besides, the strangeness chemical potentials μ_S are obtained by extrapolating the results from Ref. [85]. The values of (T, μ_B, μ_S) used in our calculation for different collision energies are listed in Table II. To model the yields of ϕ and Ω , we introduce a fugacity factor $\gamma_{s,\bar{s}}$, setting $\gamma_s = 0.65$ for 19.6–62.4 GeV and $\gamma_s = 0.8$ for 200, 2760 GeV. Note that the value of γ_s for 19.6–62.4 GeV are smaller than those obtained in thermal models [88,96]. The value of γ_s for 200, 2760 GeV is derived from quark coalescence model [71]. In order to assess the impact of γ_s , we increase the value of γ_s by 25%, setting $\gamma_s = 0.81$ for 19.6–62.4 GeV and $\gamma_s = 1$ for 200–2760 GeV, and we observe minor effects on the final results. For instance, with $\gamma_s = 0.81$ for Au+Au collisions at 62.4 GeV, the value of $\eta T/(\epsilon + P)$ decreases by only 7% and $\zeta T/(\epsilon + P)$ decreases by a mere 3% when compared to default results.

Regarding other constants, we specify the hadron wave function variances as $\sigma_M = 0.3$ and $\sigma_B = 0.1$. We have confirmed that the variations in the wave function's variances have minimal impact on our results. We use speed of sound squared $c_s^2 = 0.15$ [see Eq. (4)] for the QGP at hadronization [97,98], quark mass $m_s = 500$ MeV, spin degeneracy factor $C_M = 3$ for ϕ and $C_B = 4$ for Ω^- .

TABLE II. Values of temperature (T), baryon chemical potential (μ_B), strangeness chemical potential (μ_S), and fit ranges for ϕ and Ω observables used in quark recombination for different collision energies.

$\sqrt{s_{NN}}$ (GeV)	19.6	39	54.4	62.4	200	2760
T (MeV)	155	157.5	158.5	158.5	160	160
μ_B (MeV)	197	107	79	69	22	0
μ_S (MeV)	46	29	21	18	8	0
p_T -range (GeV/ c)	ϕ	<2.3	<2.4	<2.6	<2.7	<2.6
	Ω	<3.2	<3.0	<3.9	<3.8	<4.0

The parameters left in our model are $[\tau, \alpha_0, \alpha_2, R_y/R_x, \eta T/(\epsilon + P), \zeta T/(\epsilon + P)]$, which can be determined by Bayesian analysis of the experimental data. For each centrality bin at each collision energy, the fluid has unique values for $(\tau, \alpha_0, \alpha_2, R_y/R_x)$ and shared values for $[\eta T/(\epsilon + P), \zeta T/(\epsilon + P)]$ and thus we have $3 \times 4 + 2 = 14$ parameters for $\sqrt{s_{NN}} = 19.6\text{--}62.4$ GeV, $2 \times 4 + 2 = 10$ parameters for $\sqrt{s_{NN}} = 200$ GeV and $4 \times 4 + 2 = 18$ parameters for $\sqrt{s_{NN}} = 2.76$ TeV.

C. Bayesian method

To determine the above parameters, we employ the Bayesian analysis package from the Models and Data Analysis Initiative (MADAI) project [27,99]. The MADAI package includes a Gaussian process emulator and a Bayesian analysis tool. According to Bayes' theorem, for model parameters $x = (x_1, x_2, x_3, \dots)$ and experimental observables $y = (y_1, y_2, y_3, \dots)$, the probability for the true parameters x_* is

$$P(x_*|X, Y, y_{\text{exp}}) \propto P(X, Y, y_{\text{exp}}|x_*)P(x_*). \quad (8)$$

The left-hand side is the posterior probability of x_* given the design (X, Y) and the experimental data y_{exp} . On the right-hand side, $P(x_*)$ is the prior probability and $P(X, Y, y_{\text{exp}}|x_*)$ is the likelihood, i.e., the probability of the model describing the data y_{exp} at x_* , given by

$$P(X, Y, y_{\text{exp}}|x_*) \propto \exp\left(-\frac{1}{2}\Delta y^T \Lambda^{-1} \Delta y\right), \quad (9)$$

where $\Delta y = y_* - y_{\text{exp}}$ is the difference between the measurement and the prediction, and Λ is the covariance matrix including the experimental and model uncertainties. Further information is available in Refs. [27,30].

We adopt a uniform prior distribution for all model parameters. For instance, for 10–40% centrality bin at $\sqrt{s_{NN}} = 19.6$ GeV, we set prior ranges 5.8–7.8 fm/c for τ , 0.44–0.6c for α_0 , 0.012–0.042c for α_2 , 1.12–1.32 for R_y/R_x , and obtain posterior values $(\tau, \alpha_0, \alpha_2, R_y/R_x) = (6.8 \text{ fm/c}, 0.53c, 0.03c, 1.24)$. Besides, we set prior ranges 0–0.2 for $\eta T/(\epsilon + P)$, 0–0.12 for $\zeta T/(\epsilon + P)$ at 19.6 GeV and obtain $\eta T/(\epsilon + P) = 0.076$ and $\zeta T/(\epsilon + P) = 0.035$. The same procedure is applied to other centralities and energies.

After setting prior ranges for each parameter, we generate a set of training points within the parameter space and calculate all fitted observables at each training point. The MADAI package then builds a Gaussian process emulator, which can estimate the observables for random parameter values. Finally a Markov chain Monte Carlo (MCMC) provides a likelihood analysis and gives the maximum likelihood or best-fit parameters. Here for each collision energy we use $N = 500$ training points. To validate proper functioning of the Bayesian analysis, we perform a closure test and confirm the Bayesian framework correctly reproduces model parameters within reasonable uncertainties. The likelihood analysis has used $N_* = 2 \times 10^6$ predicted points to search for the best-fit parameters, which is sufficient for MCMC to converge.

III. RESULTS AND DISCUSSIONS

Using the data and parameters discussed earlier, we perform a model-to-data comparison with MADAI package and

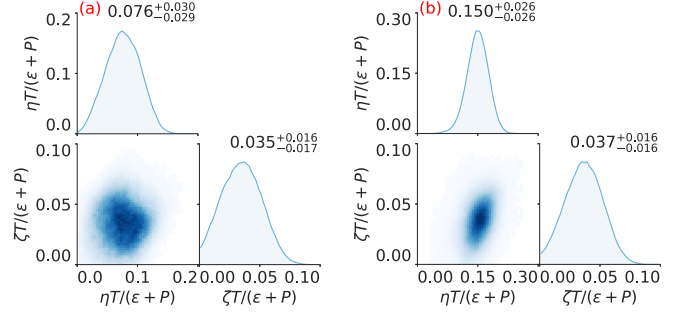


FIG. 1. Posterior distributions of $\eta T/(\epsilon + P)$ and $\zeta T/(\epsilon + P)$ for (a) Au+Au 19.6 GeV and (b) 62.4 GeV. The numbers indicate the median values with the 68.3% credibility range.

obtain the best-fit parameters, which are defined as the mean value given by the maximum likelihood analysis. As an example, we illustrate in Fig. 1 the univariate posterior distributions of η and ζ for Au+Au collisions at $\sqrt{s_{NN}} = 19.6$ GeV [Fig. 1(a)] and 62.4 GeV [Fig. 1(b)]. For 19.6 GeV, we obtain $\eta T/(\epsilon + P) = 0.076^{+0.030}_{-0.029}$ and $\zeta T/(\epsilon + P) = 0.035^{+0.017}_{-0.016}$. For 62.4 GeV, we obtain $\eta T/(\epsilon + P) = 0.15 \pm 0.026$ and $\zeta T/(\epsilon + P) = 0.037 \pm 0.016$, both at a 68.3% confidence level (C.L.). Similar results can be obtained for other collision energies.

With the best-fit parameters provided by Bayesian analysis, we can calculate transverse momentum spectra and elliptic flows of ϕ and Ω and compare with experimental data. Figure 2 shows our theoretical predictions and the corresponding experimental data for p_T spectra and v_2 of ϕ and Ω in selected centralities at different collision energies. As seen from Fig. 2, our calculations describe data rather well.

Figure 3 shows our Bayesian inference of the $\eta T/(\epsilon + P)$ [Fig. 3(a)] and $\zeta T/(\epsilon + P)$ [Fig. 3(b)] at 68.3% C.L. for the QGP at hadronization or $T \approx 160$ MeV with different μ_B . The range of baryon chemical potentials is between $\mu_B = 0$ and $\mu_B = 200$ MeV, which corresponds to collision energy varying from 2.76 TeV (most left) to 19.6 GeV (most right) [95]. For the purpose of comparison, in Fig. 3 we also include results from other approaches, i.e., Chapman-Enskog theory (Chap-Ensk) [37] for η , hadron resonance gas model (HRG) [38] and holographic model (Holo) [19] for both η and ζ . In these approaches, η and ζ are calculated as a function of temperature with different μ_B . Here we take their values at $T = 160$ MeV with $\mu_B = 0$ and $\mu_B = 300$ MeV ($T = 150$ MeV with $\mu_B = 0$ and $\mu_B = 500$ MeV for Chap-Ensk). It should be noted that the results from Chap-Ensk and HRG are for hadronic matter.

One sees from Fig. 3(a) that the shear viscosity has a significant dependency on baryon chemical potential and decreases with μ_B , which suggests that the QGP with finite baryon density is more close to perfect fluid than the baryon-free QGP. This trend of shear viscosity, i.e., $\eta T/(\epsilon + P)$ decreases as μ_B increases, aligns with observations in Chap-Ensk [37], HRG [38,40] and holographic model [19], but seems to be at variance with the findings in hybrid models [41,42,45]. We note that in the hybrid models, a constant η/s [41,42] or temperature-independent $\eta T/(\epsilon + P)$ [45] is assumed for

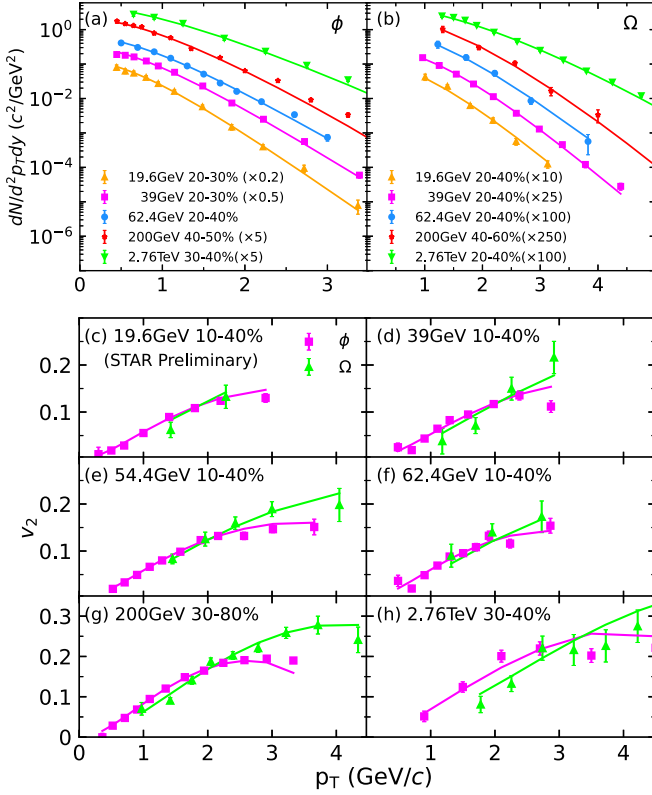


FIG. 2. Transverse-momentum spectra and elliptic flows v_2 of ϕ mesons and Ω baryons (selected centrality bins). For Au+Au at 19.6–62.4 GeV, we use data of Ω^- . For Au+Au at 200 GeV and Pb+Pb at 2.76 TeV, we use data of $\Omega^- + \bar{\Omega}^+$. Solid lines are recombination calculation using the best-fit parameters. The data from STAR [81–91] and ALICE [92–94] are included for comparison.

each collision energy and thus the obtained results are temperature averaged by neglecting the effects of varying T on viscosities of the QGP during the dynamical evolution. This is in contrast with our present results that are for QGP at hadronization with a temperature of $T \approx 160$ MeV.

It should be emphasized that the shear viscosity may have complicated dependence on the temperature and chemical potential (see, e.g., Ref. [40]). As found in Refs. [37,38], the decrease of $\eta T/(\epsilon + P)$ with μ_B is primarily attributed to the rapid increase in entropy density s and very slow increase in η with μ_B . In addition, we would like to mention that at $\mu_B = 0$, the most recent Bayesian statistical analysis leads to $\eta/s \approx 0.16$ at $T = 160$ MeV [33,36], consistent with our present result.

On the other hand, Fig. 3(b) indicates rather small ζ at hadronization for $\mu_B < 200$ MeV. In particular, we find $\zeta T/(\epsilon + P)$ is essentially constant within uncertainty with $\zeta T/(\epsilon + P) = 0.02\text{--}0.04$ for $\mu_B < 200$ MeV. Interestingly, our results are quantitatively consistent with HRG and holographic model. However, due to the limited accuracy of our results, we cannot draw any conclusions about the trend for μ_B dependence of ζ . We note that HRG predicts an increase of $\zeta T/(\epsilon + P)$ with μ_B , while the holographic model predicts an opposite behavior.

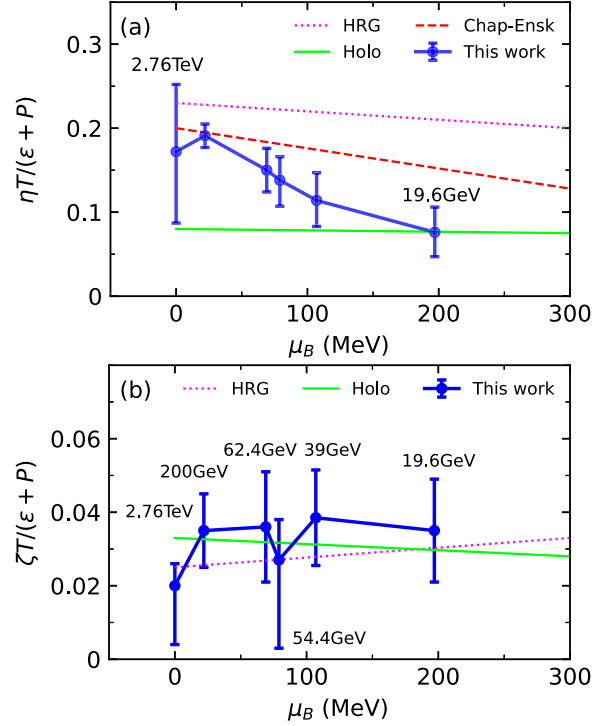


FIG. 3. Baryon chemical potential dependence of (a) shear and (b) bulk viscosities for QGP/hadronic matter at hadronization with $T \approx 160$ MeV (see text for details).

Addressing uncertainties in our analysis, we categorize them into two main groups: (i) uncertainties arising from assumptions made in the blast wave parametrization, such as the simplistic ansatz for the flow field and the recombination hypersurface, and (ii) uncertainties stemming from errors in experimental data and the quality of the Gaussian emulator. To quantify uncertainty (i), a comparison between hydro simulations and blast wave was conducted in Ref. [62] for $\mu_B = 0$ and found blast wave represents the shear stress in hydrodynamic simulations quite well, with uncertainties around 0.02 for η/s . A future exploration involving a comparison between blast wave and hydrodynamic simulations at finite μ_B is planned. Uncertainty (ii) is addressed by the MADAI code and is presented in our final results.

IV. CONCLUSIONS

We have performed Bayesian inference of the shear and bulk viscosities of the QGP at hadronization ($T \approx 160$ MeV) by analyzing the ϕ and Ω data in Au+Au collisions at $\sqrt{s_{NN}} = 19.6\text{--}200$ GeV and Pb+Pb collisions at $\sqrt{s_{NN}} = 2.76$ TeV, based on the quark recombination model coupled with a viscous blast wave. We find that the specific shear viscosity $\eta T/(\epsilon + P)$ of the QGP at hadronization decreases as μ_B increases, while the corresponding specific bulk viscosity is essentially constant for $\mu_B < 200$ MeV, suggesting that the QGP at $T \approx 160$ MeV with finite baryon density is more close to perfect fluid than that with zero baryon density.

Our work provides valuable reference for future theoretical calculations as well as parametrization of viscosities in hydrodynamic simulations for baryon-rich QGP. Our work is also useful for exploring the dynamics of binary neutron star mergers, given that quark matter is expected to exist in the cores of massive neutron stars and a transition from nuclear to quark matter may happen [100]. Furthermore, dramatic changes in transport properties may be considered as a signal of phase transition, and a thorough understanding of the baryon density dependence of viscosities of QCD matter is of great significance for the exploration of phase transition [40]. Our study represents a step forward in achieving this objective, especially if more high-quality ϕ and Ω data in Au+Au collisions at $\sqrt{s_{NN}} = 7.7$ and 11.5 GeV or

even lower collision energies would be provided at RHIC in future.

ACKNOWLEDGMENTS

The authors would like to thank R. J. Fries, D. Hou, F. Li, J. Pu, and K.-J. Sun for useful discussions. This work was supported in part by the National Natural Science Foundation of China under Grants No. 12205182, No. 12235010, No. 11625521, and No. 12375124, the National SKA Program of China Grant No. 2020SKA0120300, and the Science and Technology Commission of Shanghai Municipality under Grant No. 23JC1402700. Y.S. thanks the sponsorship from Yangyang Development Fund.

-
- [1] Z. Fodor and S. D. Katz, Critical point of QCD at finite T and μ , lattice results for physical quark masses, *J. High Energy Phys.* **04** (2004) 050.
- [2] C. Shen, Studying QGP with flow: A theory overview, *Nucl. Phys. A* **1005**, 121788 (2021).
- [3] T. Bhattacharya *et al.* (HotQCD Collaboration), QCD phase transition with chiral quarks and physical quark masses, *Phys. Rev. Lett.* **113**, 082001 (2014).
- [4] S. Borsányi, Z. Fodor, J. N. Guenther, R. Kara, S. D. Katz, P. Parotto, A. Pasztor, C. Ratti, and K. K. Szabo, QCD crossover at finite chemical potential from lattice simulations, *Phys. Rev. Lett.* **125**, 052001 (2020).
- [5] S. Borsányi, Z. Fodor, J. N. Guenther, R. Kara, S. D. Katz, P. Parotto, A. Pásztor, C. Ratti, and K. K. Szabó, Lattice QCD equation of state at finite chemical potential from an alternative expansion scheme, *Phys. Rev. Lett.* **126**, 232001 (2021).
- [6] X. An *et al.*, The BEST framework for the search for the QCD critical point and the chiral magnetic effect, *Nucl. Phys. A* **1017**, 122343 (2022).
- [7] P. K. Kovtun, D. T. Son, and A. O. Starinets, Viscosity in strongly interacting quantum field theories from black hole physics, *Phys. Rev. Lett.* **94**, 111601 (2005).
- [8] H. B. Meyer, Calculation of the shear viscosity in SU(3) gluodynamics, *Phys. Rev. D* **76**, 101701(R) (2007).
- [9] H. B. Meyer, Calculation of the bulk viscosity in SU(3) gluodynamics, *Phys. Rev. Lett.* **100**, 162001 (2008).
- [10] H. B. Meyer, Transport properties of the quark-gluon plasma from lattice QCD, *Nucl. Phys. A* **830**, 641c (2009).
- [11] S. W. Mages, S. Borsányi, Z. Fodor, A. Schäfer, and K. Szabó, Shear viscosity from lattice QCD, *PoS (LATTICE 2014)*, 232 (2015).
- [12] N. Yu. Astrakhantsev, V. V. Braguta, and A. Yu. Kotov, Temperature dependence of shear viscosity of SU(3)-gluodynamics within lattice simulation, *J. High Energy Phys.* **04** (2017) 101.
- [13] N. Y. Astrakhantsev, V. V. Braguta, and A. Y. Kotov, Temperature dependence of the bulk viscosity within lattice simulation of SU(3) gluodynamics, *Phys. Rev. D* **98**, 054515 (2018).
- [14] S. Borsányi, Z. Fodor, M. Giordano, S. D. Katz, A. Pasztor, C. Ratti, A. Schafer, K. K. Szabo, and B. C. Tóth, High statistics lattice study of stress tensor correlators in pure SU(3) gauge theory, *Phys. Rev. D* **98**, 014512 (2018).
- [15] N. Christiansen, M. Haas, J. M. Pawłowski, and N. Strodthoff, Transport coefficients in Yang–Mills theory and QCD, *Phys. Rev. Lett.* **115**, 112002 (2015).
- [16] S. Y. F. Liu and R. Rapp, Spectral and transport properties of quark–gluon plasma in a nonperturbative approach, *Eur. Phys. J. A* **56**, 44 (2020).
- [17] J. Ghiglieri, G. D. Moore, and D. Teaney, QCD shear viscosity at (almost) NLO, *J. High Energy Phys.* **03** (2018) 179.
- [18] R. Rougemont, R. Critelli, J. Noronha-Hostler, J. Noronha, and C. Ratti, Dynamical versus equilibrium properties of the QCD phase transition: A holographic perspective, *Phys. Rev. D* **96**, 014032 (2017).
- [19] J. Grefa, M. Hippert, J. Noronha, J. Noronha-Hostler, I. Portillo, C. Ratti, and R. Rougemont, Transport coefficients of the quark-gluon plasma at the critical point and across the first-order line, *Phys. Rev. D* **106**, 034024 (2022).
- [20] D. Teaney, The effects of viscosity on spectra, elliptic flow, and HBT radii, *Phys. Rev. C* **68**, 034913 (2003).
- [21] S. Ryu, J. F. Paquet, C. Shen, G. S. Denicol, B. Schenke, S. Jeon, and C. Gale, Importance of the bulk viscosity of QCD in ultrarelativistic heavy-ion collisions, *Phys. Rev. Lett.* **115**, 132301 (2015).
- [22] P. Romatschke and U. Romatschke, Viscosity information from relativistic nuclear collisions: How perfect is the fluid observed at RHIC? *Phys. Rev. Lett.* **99**, 172301 (2007).
- [23] B. Schenke, S. Jeon, and C. Gale, Elliptic and triangular flow in event-by-event $D = 3 + 1$ viscous hydrodynamics, *Phys. Rev. Lett.* **106**, 042301 (2011).
- [24] C. Gale, S. Jeon, B. Schenke, P. Tribedy, and R. Venugopalan, Event-by-event anisotropic flow in heavy-ion collisions from combined Yang–Mills and viscous fluid dynamics, *Phys. Rev. Lett.* **110**, 012302 (2013).
- [25] H. Niemi, K. J. Eskola, and R. Paatelainen, Event-by-event fluctuations in a perturbative QCD + saturation + hydrodynamics model: Determining QCD matter shear viscosity in ultrarelativistic heavy-ion collisions, *Phys. Rev. C* **93**, 024907 (2016).
- [26] J. E. Bernhard, P. W. Marcy, C. E. Coleman-Smith, S. Huzurbazar, R. L. Wolpert, and S. A. Bass, Quantifying properties of hot and dense QCD matter through systematic model-to-data comparison, *Phys. Rev. C* **91**, 054910 (2015).

- [27] J. E. Bernhard, J. S. Moreland, S. A. Bass, J. Liu, and U. Heinz, Applying Bayesian parameter estimation to relativistic heavy-ion collisions: Simultaneous characterization of the initial state and quark-gluon plasma medium, *Phys. Rev. C* **94**, 024907 (2016).
- [28] J. E. Bernhard, J. S. Moreland, and S. A. Bass, Bayesian estimation of the specific shear and bulk viscosity of quark-gluon plasma, *Nat. Phys.* **15**, 1113 (2019).
- [29] D. Everett *et al.* (JETSCAPE Collaboration), Phenomenological constraints on the transport properties of QCD matter with data-driven model averaging, *Phys. Rev. Lett.* **126**, 242301 (2021).
- [30] D. Everett *et al.* (JETSCAPE Collaboration), Multisystem Bayesian constraints on the transport coefficients of QCD matter, *Phys. Rev. C* **103**, 054904 (2021).
- [31] G. Nijs, W. van der Schee, U. Gürsoy, and R. Snellings, Transverse momentum differential global analysis of heavy-ion collisions, *Phys. Rev. Lett.* **126**, 202301 (2021).
- [32] G. Nijs, W. van der Schee, U. Gürsoy, and R. Snellings, Bayesian analysis of heavy ion collisions with the heavy ion computational framework Trajectum, *Phys. Rev. C* **103**, 054909 (2021).
- [33] G. Nijs and W. van der Schee, Hadronic nucleus-nucleus cross section and the nucleon size, *Phys. Rev. Lett.* **129**, 232301 (2022).
- [34] J. E. Parkkila, A. Onnerstad, and D. J. Kim, Bayesian estimation of the specific shear and bulk viscosity of the quark-gluon plasma with additional flow harmonic observables, *Phys. Rev. C* **104**, 054904 (2021).
- [35] J. E. Parkkila, A. Onnerstad, S. F. Taghavi, C. Mordasini, A. Bilandzic, M. Virta, and D. J. Kim, New constraints for QCD matter from improved Bayesian parameter estimation in heavy-ion collisions at LHC, *Phys. Lett. B* **835**, 137485 (2022).
- [36] M. R. Heffernan, C. Gale, S. Jeon, and J.-F. Paquet, Bayesian quantification of strongly-interacting matter with color glass condensate initial conditions, [arXiv:2302.09478](https://arxiv.org/abs/2302.09478).
- [37] G. S. Denicol, C. Gale, S. Jeon, and J. Noronha, Fluid behavior of a baryon-rich hadron resonance gas, *Phys. Rev. C* **88**, 064901 (2013).
- [38] G. P. Kadam and H. Mishra, Dissipative properties of hot and dense hadronic matter in an excluded-volume hadron resonance gas model, *Phys. Rev. C* **92**, 035203 (2015).
- [39] O. Soloveva, D. Fuseau, J. Aichelin, and E. Bratkovskaya, Shear viscosity and electric conductivity of a hot and dense QGP with a chiral phase transition, *Phys. Rev. C* **103**, 054901 (2021).
- [40] E. McLaughlin, J. Rose, T. Dore, P. Parotto, C. Ratti, and J. Noronha-Hostler, Building a testable shear viscosity across the QCD phase diagram, *Phys. Rev. C* **105**, 024903 (2022).
- [41] I. A. Karpenko, P. Huovinen, H. Petersen, and M. Bleicher, Estimation of the shear viscosity at finite net-baryon density from $A + A$ collision data at $\sqrt{s_{NN}} = 7.7 - 200$ GeV, *Phys. Rev. C* **91**, 064901 (2015).
- [42] J. Auvinen, J. E. Bernhard, S. A. Bass, and I. Karpenko, Investigating the collision energy dependence of η/s in the beam energy scan at the BNL relativistic heavy ion collider using Bayesian statistics, *Phys. Rev. C* **97**, 044905 (2018).
- [43] C. Shen and S. Alzhrani, Collision-geometry-based 3D initial condition for relativistic heavy-ion collisions, *Phys. Rev. C* **102**, 014909 (2020).
- [44] N. Götz and H. Elfner, Temperature and net baryochemical potential dependence of η/s in a hybrid approach, *Phys. Rev. C* **106**, 054904 (2022).
- [45] C. Shen, B. Schenke, and W. Zhao, Viscosities of the baryon-rich quark-gluon plasma from beam energy scan data, *Phys. Rev. Lett.* **132**, 072301 (2024).
- [46] Y. Akamatsu, M. Asakawa, T. Hirano, M. Kitazawa, K. Morita, K. Murase, Y. Nara, C. Nonaka, and A. Ohnishi, Dynamically integrated transport approach for heavy-ion collisions at high baryon density, *Phys. Rev. C* **98**, 024909 (2018).
- [47] L. Du and U. Heinz, (3+1)-dimensional dissipative relativistic fluid dynamics at non-zero net baryon density, *Comput. Phys. Commun.* **251**, 107090 (2020).
- [48] X.-Y. Wu, G.-Y. Qin, L.-G. Pang, and X.-N. Wang, (3+1)-D viscous hydrodynamics at finite net baryon density: Identified particle spectra, anisotropic flows, and flow fluctuations across energies relevant to the beam-energy scan at RHIC, *Phys. Rev. C* **105**, 034909 (2022).
- [49] Z. Yang and L.-W. Chen, Bayesian inference of the specific shear and bulk viscosities of the quark-gluon plasma at crossover from ϕ and Ω observables, *Phys. Rev. C* **107**, 064910 (2023).
- [50] V. Greco, C. M. Ko, and P. Levai, Parton coalescence and anti-proton/pion anomaly at RHIC, *Phys. Rev. Lett.* **90**, 202302 (2003).
- [51] V. Greco, C. M. Ko, and P. Levai, Parton coalescence at RHIC, *Phys. Rev. C* **68**, 034904 (2003).
- [52] R. J. Fries, B. Muller, C. Nonaka, and S. A. Bass, Hadronization in heavy ion collisions: Recombination and fragmentation of partons, *Phys. Rev. Lett.* **90**, 202303 (2003).
- [53] R. J. Fries, B. Muller, C. Nonaka, and S. A. Bass, Hadron production in heavy ion collisions: Fragmentation and recombination from a dense parton phase, *Phys. Rev. C* **68**, 044902 (2003).
- [54] R. C. Hwa and C. B. Yang, Scaling behavior at high p_T and the p/π ratio, *Phys. Rev. C* **67**, 034902 (2003).
- [55] L.-W. Chen, C. M. Ko, and Z.-W. Lin, Partonic effects on high order anisotropic flows in relativistic heavy ion collisions, *Phys. Rev. C* **69**, 031901(R) (2004).
- [56] P. F. Kolb, L.-W. Chen, V. Greco, and C. M. Ko, Momentum anisotropies in the quark coalescence model, *Phys. Rev. C* **69**, 051901(R) (2004).
- [57] R. J. Fries, V. Greco, and P. Sorensen, Coalescence models for hadron formation from quark gluon plasma, *Annu. Rev. Nucl. Part. Sci.* **58**, 177 (2008).
- [58] M. He, R. J. Fries, and R. Rapp, Scaling of elliptic flow, recombination and sequential freeze-out of hadrons in heavy-ion collisions, *Phys. Rev. C* **82**, 034907 (2010).
- [59] W. Zhao, C. M. Ko, Y.-X. Liu, G.-Y. Qin, and H. Song, Probing the partonic degrees of freedom in high-multiplicity $p - Pb$ collisions at $\sqrt{s_{NN}} = 5.02$ TeV, *Phys. Rev. Lett.* **125**, 072301 (2020).
- [60] A. Jaiswal and V. Koch, A viscous blast-wave model for relativistic heavy-ion collisions, [arXiv:1508.05878](https://arxiv.org/abs/1508.05878).

- [61] Z. Yang and R. J. Fries, A blast wave model with viscous corrections, *J. Phys.: Conf. Ser.* **832**, 012056 (2017).
- [62] Z. Yang and R. J. Fries, Parameterizing smooth viscous fluid dynamics with a viscous blast wave, *J. Phys. G* **51**, 015102 (2024).
- [63] Z. Yang and R. J. Fries, Shear stress tensor and specific shear viscosity of hot hadron gas in nuclear collisions, *Phys. Rev. C* **105**, 014910 (2022).
- [64] A. Shor, Phi meson production as a probe of the quark-gluon plasma, *Phys. Rev. Lett.* **54**, 1122 (1985).
- [65] H. van Hecke, H. Sorge, and N. Xu, Evidence of early multistrange hadron freezeout in high-energy nuclear collisions, *Phys. Rev. Lett.* **81**, 5764 (1998).
- [66] L.-W. Chen and C. M. Ko, ϕ and Ω production from relativistic heavy ion collisions in a dynamical quark coalescence model, *Phys. Rev. C* **73**, 044903 (2006).
- [67] J. H. Chen, F. Jin, D. Gangadharan, X. Z. Cai, H. Z. Huang, and Y. G. Ma, Parton distributions at hadronization from bulk dense matter produced at RHIC, *Phys. Rev. C* **78**, 034907 (2008).
- [68] J. Auvinen, K. Redlich, and S. A. Bass, Multi-strange hadrons and the precision extraction of QGP properties in the RHIC-BES domain, *J. Phys.: Conf. Ser.* **779**, 012045 (2017).
- [69] R. C. Hwa and L. Zhu, Phenomenological implications of the p_T spectra of ϕ and Ω produced at LHC and RHIC, *J. Phys.: Conf. Ser.* **779**, 012049 (2017).
- [70] Y. J. Ye, J. H. Chen, Y. G. Ma, S. Zhang, and C. Zhong, Ω and ϕ in Au + Au collisions at $\sqrt{s_{NN}} = 200$ and 11.5 GeV from a multiphase transport model, *Chin. Phys. C* **41**, 084101 (2017).
- [71] J. Pu, K.-J. Sun, and L.-W. Chen, Extracting strange quark freeze-out information in Pb+Pb collisions at $\sqrt{s_{NN}} = 2.76$ TeV from ϕ and Ω production, *Phys. Rev. C* **98**, 064905 (2018).
- [72] J. Song, F. L. Shao, and Z. T. Liang, Quark number scaling of p_T spectra for Ω and ϕ in relativistic heavy-ion collisions, *Phys. Rev. C* **102**, 014911 (2020).
- [73] F. Retiere and M. A. Lisa, Observable implications of geometrical and dynamical aspects of freeze out in heavy ion collisions, *Phys. Rev. C* **70**, 044907 (2004).
- [74] H. Song and U. W. Heinz, Causal viscous hydrodynamics in 2+1 dimensions for relativistic heavy-ion collisions, *Phys. Rev. C* **77**, 064901 (2008).
- [75] M. Damodaran, D. Molnar, G. G. Barnaföldi, D. Berényi, and M. F. Nagy-Egri, Improved single-particle phase-space distributions for viscous fluid dynamic models of relativistic heavy ion collisions, *Phys. Rev. C* **102**, 014907 (2020).
- [76] G. S. Denicol, S. Jeon, and C. Gale, Transport coefficients of bulk viscous pressure in the 14-moment approximation, *Phys. Rev. C* **90**, 024912 (2014).
- [77] J.-F. Paquet, C. Shen, G. S. Denicol, M. Luzum, B. Schenke, S. Jeon, and C. Gale, Production of photons in relativistic heavy-ion collisions, *Phys. Rev. C* **93**, 044906 (2016).
- [78] J. Liao and V. Koch, On the fluidity and super-criticality of the QCD matter at RHIC, *Phys. Rev. C* **81**, 014902 (2010).
- [79] B. Abelev *et al.* (ALICE Collaboration), Centrality determination of Pb-Pb collisions at $\sqrt{s_{NN}} = 2.76$ TeV with ALICE, *Phys. Rev. C* **88**, 044909 (2013).
- [80] HADES Collaboration, J. Adamczewski-Musch *et al.*, Centrality determination of Au + Au collisions at 1.23A GeV with HADES, *Eur. Phys. J. A* **54**, 85 (2018).
- [81] L. Adamczyk *et al.* (STAR Collaboration), Centrality dependence of identified particle elliptic flow in relativistic heavy ion collisions at $\sqrt{s_{NN}} = 7.7 - 62.4$ GeV, *Phys. Rev. C* **93**, 014907 (2016).
- [82] Li-Ke Liu (for the STAR Collaboration), Elliptic and triangular flow of (multi-) strange hadrons and phi mesons in BES-II energies at STAR, *EPJ Web Conf.* **276**, 01018 (2023).
- [83] P. Dixit (for the STAR collaboration), Anisotropic flow of (multi-) strange hadrons in Au+Au collisions at BES-II energies, *PoS (ICHEP2022)*, 496 (2022).
- [84] L. Adamczyk *et al.* (STAR Collaboration), Probing parton dynamics of QCD matter with Ω and ϕ production, *Phys. Rev. C* **93**, 021903 (2016).
- [85] J. Adam *et al.* (STAR Collaboration), Strange hadron production in Au+Au collisions at $\sqrt{s_{NN}} = 7.7, 11.5, 19.6, 27,$ and 39 GeV, *Phys. Rev. C* **102**, 034909 (2020).
- [86] M. S. Abdallah *et al.* (STAR Collaboration), Azimuthal anisotropy measurement of (multi)strange hadrons in Au+Au collisions at $\sqrt{s_{NN}} = 54.4$ GeV, *Phys. Rev. C* **107**, 024912 (2023).
- [87] B. I. Abelev *et al.* (STAR Collaboration), Measurements of phi meson production in relativistic heavy-ion collisions at RHIC, *Phys. Rev. C* **79**, 064903 (2009).
- [88] M. M. Aggarwal *et al.* (STAR Collaboration), Strange and multi-strange particle production in Au+Au collisions at $\sqrt{s_{NN}} = 62.4$ GeV, *Phys. Rev. C* **83**, 024901 (2011), [Erratum: **107**, 049903(E) (2023)].
- [89] M. M. Aggarwal *et al.* (STAR Collaboration), Centrality and transverse momentum dependence of elliptic flow of multistrange hadrons and ϕ meson in Au+Au collisions at $\sqrt{s_{NN}} = 200$ GeV, *Phys. Rev. Lett.* **116**, 062301 (2016).
- [90] J. Adams *et al.* (STAR Collaboration), Scaling properties of hyperon production in Au+Au collisions at $\sqrt{s_{NN}} = 200$ GeV, *Phys. Rev. Lett.* **98**, 062301 (2007).
- [91] B. I. Abelev *et al.* (STAR Collaboration), Partonic flow and phi-meson production in Au + Au collisions at $\sqrt{s_{NN}} = 200$ GeV, *Phys. Rev. Lett.* **99**, 112301 (2007).
- [92] The ALICE Collaboration, B. B. Abelev *et al.*, Elliptic flow of identified hadrons in Pb-Pb collisions at $\sqrt{s_{NN}} = 2.76$ TeV, *J. High Energy Phys.* **06** (2015) 190.
- [93] J. Adam *et al.* (ALICE Collaboration), Corrigendum to $K^*(892)^0$ and $\phi(1020)$ meson production at high transverse momentum in pp and Pb-Pb collisions at $\sqrt{s_{NN}} = 2.76$ TeV, *Phys. Rev. C* **95**, 064606 (2017).
- [94] ALICE Collaboration, B. B. Abelev *et al.*, Multi-strange baryon production at mid-rapidity in Pb-Pb collisions at $\sqrt{s_{NN}} = 2.76$ TeV, *Phys. Lett. B* **728**, 216 (2014), [Erratum: **734**, 409(E) (2014)].
- [95] A. Andronic, P. Braun-Munzinger, K. Redlich, and J. Stachel, Decoding the phase structure of QCD via particle production at high energy, *Nature* **561**, 321 (2018).
- [96] L. Adamczyk *et al.* (STAR Collaboration), Bulk properties of the medium produced in relativistic heavy-ion collisions from the beam energy scan program, *Phys. Rev. C* **96**, 044904 (2017).

- [97] P. Huovinen and P. Petreczky, QCD equation of state and hadron resonance gas, *Nucl. Phys. A* **837**, 26 (2010).
- [98] A. Monnai, B. Schenke, and C. Shen, Equation of state at finite densities for QCD matter in nuclear collisions, *Phys. Rev. C* **100**, 024907 (2019).
- [99] S. A. Bass *et al.* (MADAI Collaboration), <http://madai.phy.duke.edu/>, accessed June, 2016.
- [100] E. R. Most, L. J. Papenfort, V. Dexheimer, M. Hanauske, S. Schramm, H. Stöcker, and L. Rezzolla, Signatures of quark-hadron phase transitions in general-relativistic neutron-star mergers, *Phys. Rev. Lett.* **122**, 061101 (2019).